Journal of Solid State Chemistry **151,** 231–240 (2000)
doi:10.1006/jssc.2000.8645, available online at http://www.idealibrary.com on IDEAL®

Pressure-Induced Structural Phase Transitions in $Ln_{2-x}Nd_xCuO_4$ for $Ln = La$ ($0.6 \leq x \leq 2$) and $Ln = Pr$ ($x = 0$)

H. Wilhelm[1]

Département de Physique de la Matière Condensée, Université de Genève, 24, Quai Ernest-Ansermet, CH-1211 Geneva 4, Switzerland

C. Cros, E. Reny, and G. Demazeau

Institut de Chimie de la Matière Condensée de Bordeaux, UPR-CNRS 9048, 87, Avenue Dr. Albert Schweitzer, F-33608 Pessac Cedex, France

and

M. Hanfland

European Synchrotron Radiation Facility, B.P. 220, F-38043 Grenoble Cedex, France

Received October 14, 1999; in revised form January 25, 2000; accepted February 3, 2000

We have investigated the structural properties of $LaNdCuO_4$ and Pr_2CuO_4 under hydrostatic pressure up to 37 GPa at ambient temperature by high-resolution angle-dispersive X-ray powder diffraction. Upon increasing pressure a structural transformation into the T-structure (*I*4/*mmm*, K_2NiF_4-type) was observed at $P_T = 11.4$ GPa and $P_T = 15.1$ GPa, respectively. Full-profile refinements of the diffraction data give evidence for a gradual distortion of the T-structure into the orthorhombic O-phase (*Cmca*, distorted K_2NiF_4-type) during pressure release in a certain pressure interval. At low pressures the initial T′-structure (*I*4/*mmm*, Nd_2CuO_4-type) is eventually recovered again. The axis and volume compressibilities are well described by a simple model that considers the linear compressibilities of different polyhedra building the unit-cell. The occurrence of the O-phase can be understood within the tolerance factor *t* versus P_T phase diagram. © 2000 Academic Press

1. INTRODUCTION

La_2CuO_4 and Nd_2CuO_4 are the compounds of the hole- and electron-doped high–T_c superconductors $La_{2-z}Sr_zCuO_4$ and $Nd_{2-y}Ce_yCuO_4$. $La_{2-z}Sr_zCuO_4$ is the simplest copper-oxide superconductor and its systematic study has revealed an evolution from an antiferromagnetic (AFM) insulator to a normal metal via a superconducting state ($0.07 \leq z \leq 0.24$; $T_c \approx 36$ K for $z = 0.15$ (1)). The AFM order is caused by the Cu-moments which are ordered below $T_N = 320$ K (2). The crystal structure is orthorhombic (*Cmca*) and contains distorted [CuO_6] octahedra (Fig. 1b). The CuO_2 planes are buckled to relieve compressive stress on them caused by the mismatch of (La,Sr)–O and Cu–O bonds. As z exceeds 0.21, a structural transition into the tetragonal T-structure occurs (*I*4/*mmm*, K_2NiF_4-type, Fig. 1c) and simultaneously the superconducting transition temperature T_c decreases sharply (1, 3). Measurements on samples with $z \leq 0.18$ under hydrostatic pressure showed that T_c increases linearly with pressure but does not vary as soon as the tetragonal phase is induced by pressure (4, 5). This change in $\partial T_c/\partial P$ is believed to be related with the orthorhombic–tetragonal transition (3) and thus, the maximum in T_c occurs when the CuO_2 planes are flat or almost flat. Furthermore, pressure experiments on $La_{2-z}Sr_zCuO_4$ ($z = 0.10$ and $z = 0.15$) have shown that T_c varies inversely with the tilt angle and is maximum in the tetragonal structure, i.e., with flat and square CuO_2 planes (6).

An interesting difference to the magnetic properties of the compounds mentioned so far is found for the parent compound of the electron-doped superconductors $R_{2-y}Ce_yCuO_4$ (R = Pr and Nd) (7). In Nd_2CuO_4 (T′- structure, *I*4/*mmm*, Fig. 1a) several magnetic phases occur as the temperature is lowered or a magnetic field is applied. Furthermore, the magnetic moment of the Nd^{3+} is able both to interact with (next nearest) Cu spins and to order spontaneously at low temperature (Ref. (8) and references therein). Below 30 K the Cu moments are oriented antiferromagnetically along the *a*-axis as well as in the basal plane of the tetragonal structure. Along the *c*-axis adjacent Cu spins are coupled ferromagnetically. The same order occurs for the Nd sublattice below 5 K. Neighboring Nd and Cu spins

[1] To whom correspondence should be addressed. E-mail: Heribert.Wilhelm@physics.unige.ch.

0022-4596/00 $35.00

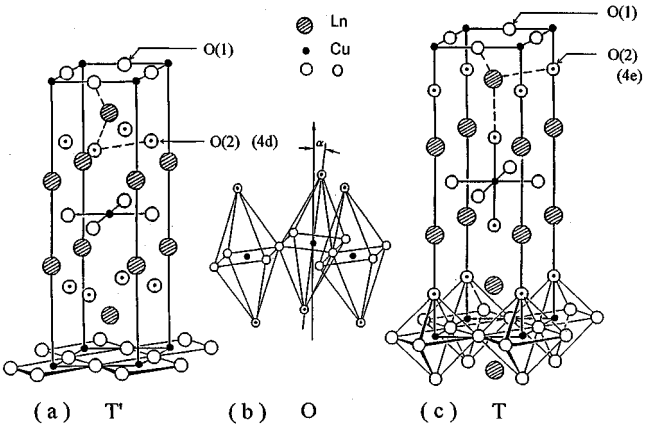

FIG. 1. Schematic view of the different crystal structures attained by the compounds of the $La_{2-x}Nd_xCuO_4$ solid–solution ($0.6 \leq x \leq 2.0$) and Pr_2CuO_4 at different pressures. (a) The low pressure T′-phase (*I*4/*mmm*, Nd_2CuO_4-type), (b) the intermediate orthorhombic O-phase (*Cmca*, distorted K_2NiF_4-type), and (c) the high pressure T-phase (*I*4/*mmm*, K_2NiF_4-type).

are coupled ferromagnetically. In the $Nd_{1.85}Ce_{0.15}CuO_4$ superconductor the Cu spins are not ordered but the Nd-sublattice shows the same magnetic order (below 1.2 K) as in Nd_2CuO_4 (9). Thus, magnetic order and superconductivity coexist. In addition, heavy-fermion behavior below 1 K was found for a doping range $0.15 \leq y \leq 0.2$ (10). According to theoretical considerations (11), the low temperature state of $Nd_{1.85}Ce_{0.15}CuO_4$ is a new prototype of a heavy-fermion system, where the Nd moments interact with strongly correlated electrons at the Cu site.

In the context of these various ground states in combination with the structural transitions it is worthwhile to study in detail the pressure-induced structural changes of the T′-structure attained by $LaNdCuO_4$ and Pr_2CuO_4. This will deliver additional information about the phase sequence, axis and volume compressibilities, and the pressure dependence of the *Ln*–O and Cu–O distances.

Recent investigations of the evolution of the T′-structure for the solid-solution $La_{2-x}Nd_xCuO_4$ ($0.6 \leq x \leq 2.0$) under pressure (12, 13) showed that the transition into the T-structure occurs at a pressure P_T. The increase of P_T with x was related to compressive stress in the *Ln*–O_2 linkages of the fluorite-type LnO_2 layers in the T′-structure. The compressive stress decreases when the average lanthanide ion size is reduced, i.e., $x \to 2$. Furthermore, the pressure effects were also described in terms of a pressure dependent tolerance factor t. It was found that the transition pressure P_T increases as t decreases.

This article is organized as follows. In Section 2 the sample preparation and the high-pressure technique are reported. The structural investigation of $LaNdCuO_4$ and Pr_2CuO_4 up to 37 GPa using synchrotron radiation are presented in Section 3. In Section 4 a simple model is introduced to calculate the axis and volume compressibilities which are then compared to those obtained by the measurements. Furthermore, the structural evolution with pressure is discussed using the relation between P_T and the tolerance factor t.

2. EXPERIMENTAL

The polycrystalline sample of $LaNdCuO_4$ was synthesized by a co-precipitation method. Stoichiometric amounts of the oxides CuO, La_2O_3, and Nd_2O_3 were separately dissolved in hot solutions of HNO_3, which were then cooled to ambient temperature and diluted with water. The La^{3+} and Nd^{3+} solutions were mixed together and poured simultaneously with the Cu^{2+} one in a solution of potassium carbonate in excess. After decantation, the precipitate was filtered and carefully washed with water. After drying at 110°C and grinding, the resulting mixture was reacted twice at 850°C for 24 h with an intermediate grinding. A similar process was used to synthesize Pr_2CuO_4, except that the starting rare earth oxide was Pr_6O_{11} and that the high-temperature reactions were carried out under nitrogen atmosphere instead of air. The resulting products were identified by X-ray diffraction, using a conventional powder diffractometer (Cu$K\alpha$ and $\theta < 70°$).

The high-pressure experiments were performed at ambient temperature using a membrane-type diamond anvil cell (DAC). A well-powdered specimen was filled into a 0.125 mm bore, which was drilled into a stainless steel gasket. The gasket was placed between the two diamonds of the DAC. Nitrogen served as pressure transmitting medium. This ensured quasi-hydrostatic pressure conditions up to the highest pressure. The pressure was determined with the ruby luminescence technique (14) and the nonlinear ruby pressure scale (15, 16). Under these circumstances the experimental error in the pressure was less than 0.2 GPa.

The X-ray powder diffraction spectra were recorded at the beamline ID09 at the European Synchrotron Radiation Facility. The high X-ray flux of the synchrotron combined with the image plate (size A3) provides a much better resolution than the technique used in the former investigation (12). The diffraction images were collected at a wavelength of $\lambda = 0.46053$ Å ($E \approx 27$ keV) during 60 s exposure time. The images were integrated with the program *fit2d* (17). The structural parameters and interionic distances were obtained by Rietveld refinement (18) of the diffraction patterns. The coexistence of two phases was taken into account by adjusting a phase fraction parameter. In any case the new phase was chosen to be higher symmetric (T′- or T-phase) as long as no clear splitting of some lines (caused by the orthorhombic symmetry) was obvious or the *R*-values were improved considerably.

Furthermore, isotropic temperature factors were used. Those of the *Ln* and Cu atoms and those of the oxygen

atoms were kept the same and these two parameters were refined independently. All refinements gave R_{wp} values between 2 and 6% depending on the pressure where the pattern was obtained. As diffraction lines of solid N_2 occurred they were refined too. Depending on pressure, the known high-pressure phases of solid N_2 were used (see e.g., Ref. (19) and references therein) but in the diffraction patterns shown below, the corresponding Bragg peak positions are not indicated.

3. RESULTS

Two diffraction patterns of $LaNdCuO_4$ recorded at low and high pressure are shown in Fig. 2. The low-pressure phase is well described within the T′-structure (Fig. 2a) but at $P_T = 11.4$ GPa a structural change into the high-pressure T-phase occurs. Above 15 GPa only the T-phase is present as can be seen in Fig. 2b. It is already mentioned here that

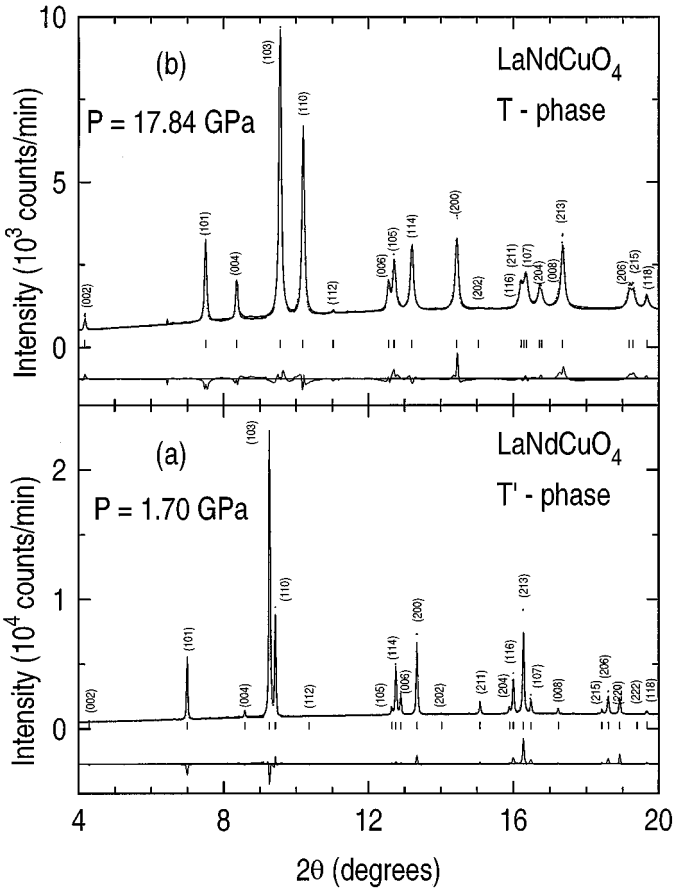

FIG. 2. Powder diffraction, refined, and difference pattern as well as Bragg peak positions of (a) the low pressure T′-phase and (b) the high pressure T-phase of $LaNdCuO_4$. In both cases the lines are indexed according to the $I4/mmm$ space group symmetry. At high pressure N_2-lines (due to the pressure transmitting medium) were refined too, but are not shown.

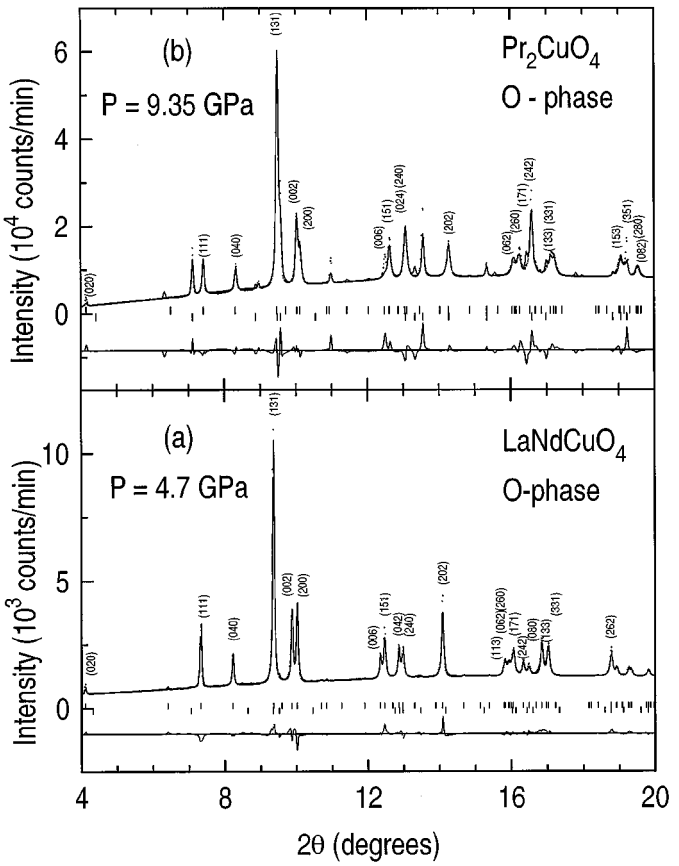

FIG. 3. Powder diffraction, refined, and difference pattern as well as Bragg peak positions of (a) $LaNdCuO_4$ and (b) Pr_2CuO_4 obtained upon pressure release. A splitting of several lines is a clear sign of an orthorhombic O-phase (*Cmca*). In both cases the patterns contain traces of the T′-phase. Only the strongest peaks of the O-phase are indexed according to the *Cmca* space group symmetry. The peaks of solid N_2 (caused by the pressure transmitting medium) were refined too, but are not shown.

a certain pressure range exists, where both the T′- and the T-phase coexist. In the case of $LaNdCuO_4$ a continuous increase in the T-phase fraction was observed in a pressure range extending 4 GPa above the phase transition pressure P_T. The structural transition becomes evident if the relative position of some lines are compared to the low-pressure phase, for example, the lines (103) and (110), (114) and (200) or (213) and (107). The structural changes are due to a shift of the O(2)-ions from the 4*d* position in the T′-structure ($I4/mmm$) to the 4*e* site in the T-phase ($I4/mmm$) (see Fig. 1).

Upon releasing pressure a two phase mixture of T- and T′-phase exists in a certain pressure range just above P_T. At 10.6 GPa some lines of the T-phase, e.g., (110), (114), and (213), split gradually, indicating another structural transition into a lower symmetric phase. Figure 3a shows the pattern of $LaNdCuO_4$, recorded at $P = 4.7$ GPa, where these splittings are evident. The orthorhombic O-phase gives a good description of the patterns as can be seen from

the low residuals (20). Thus, the mixture of O- and T′-phase was used for pressures down to $P = 2.35$ GPa. At lower pressures the initial T′-structure was completely recovered again. It is mentioned that this coexistence is only clearly visible in the pattern recorded below 4.7 GPa. At higher pressures only the slightly enlarged width of some lines, especially the (131) line, has been interpreted as a sign for the coexistence of the T′- and O-phase.

The same phase sequence was also observed for Pr_2CuO_4 (21). First signs of the T-phase were found above $P_T = 15.1$ GPa. But up to the highest pressure (37.2 GPa) no complete transformation was achieved and the T′-phase fraction was still 50%. During pressure release the splitting of some lines, as in the case of $LaNdCuO_4$, became evident below 12.6 GPa. However, this splitting was never as clear as in $LaNdCuO_4$ (see Fig. 3b). Details of the full-profile refinement of the diffraction data of $LaNdCuO_4$ and for Pr_2CuO_4, respectively, are given in Tables 1 and 2 (22). Table 3 gives an overview of the phase transition pressures, the pressure range where the T′- and T-phase (T′- and O-phase) coexist in the three compounds measured so far with synchrotron radiation.

TABLE 1
Lattice Parameters, Unit-Cell Volume, Fractional Coordinates, and Temperature Factors of $LaNdCuO_4$ in the T′-, T-, and O-Structure, Respectively

$LaNdCuO_4$	*I*4/*mmm* T′ ($Z = 2$) $P = 10^{-4}$ GPa	*I*4/*mmm* T ($Z = 2$) $P_T = 11.4$ GPa	*Cmca* O ($Z = 4$) $P = 8.0$ GPa
a (Å)	3.9746(1)	3.6990(2)	5.2431(2)
b (Å)	3.9746(1)	3.6990(2)	12.7848(7)
c (Å)	12.3647(4)	12.724(2)	5.2931(3)
V (Å^3)	195.328(7)	174.10(3)	354.82(2)
La/Nd x/a	0	0	0
y/b	0	0	0.1392(1)
z/c	0.3506(2)	0.3640(2)	0.4898(1)
U(100 Å^2)	2.72(1)	1.76(8)	0.5(1)
Cu x/a	0	0	0
y/b	0	0	0.5
z/c	0	0	0.5
U (100 Å^2)	2.72(1)	1.76(8)	0.5(1)
O(1) x/a	0	0	0.25
y/b	0.5	0.5	0.516(2)
z/c	0	0	0.25
U(100 Å^2)	1.2(1)	2.8(4)	9.2(2)
O(2) x/a	0	0	0
y/b	0.5	0	0.318(1)
z/c	0.25	0.176(2)	0.489(7)
U(100 Å^2)	1.2(1)	2.8(4)	9.2(2)
R_{wp} (%)	5.5	3.9	4.4

Note. The number of formula units per unit-cell volume is labeled with Z. The given pressure for the orthorhombic phase is the lowest pressure at which this phase was observed during pressure release. Numbers in parentheses represent standard deviations of the last digit.

TABLE 2
Lattice Parameters, Unit-Cell Volume, Fractional Coordinates, and Temperature Factors of Pr_2CuO_4 in the T′-, T-, and O-Structure, Respectively

Pr_2CuO_4	*I*4/*mmm* T′ ($Z = 2$) $P = 10^{-4}$ GPa	*I*4/*mmm* T ($Z = 2$) $P = 18.0$ GPa	*Cmca* O ($Z = 4$) $P = 5.8$ GPa
a (Å)	3.9609(1)	3.654(8)	5.250(2)
b (Å)	3.9609(1)	3.654(8)	12.748(5)
c (Å)	12.2395(3)	12.546(7)	5.319(2)
V (Å^3)	192.026(6)	167.51(9)	356.0(2)
Pr x/a	0	0	0
y/b	0	0	0.134(1)
z/c	0.3531(1)	0.3658(9)	0.484(6)
U(100 Å^2)	0.3(1)	2.9(5)	2.0(9)
Cu x/a	0	0	0
y/b	0	0	0.5
z/c	0	0	0.5
U(100 Å^2)	0.3(1)	2.9(5)	2.0(9)
O(1) x/a	0	0	0.25
y/b	0.5	0.5	0.418(9)
z/c	0	0	0.25
U(100 Å^2)	2.6(4)	2.7(6)	4 (1)
O(2) x/a	0	0	0
y/b	0.5	0	0.329(7)
z/c	0.25	0.17(1)	0.50(4)
U(100 Å^2)	2.6(4)	2.7(6)	4 (1)
R_{wp} (%)	4.0	3.1	4.0

Note. The number of formula units per unit-cell volume is labeled with Z. The given pressure for the orthorhombic phase is the lowest pressure at which this phase was observed during pressure release. Numbers in parentheses represent standard deviations of the last digit.

The pressure dependence of the relative volume V/V_0 for $LaNdCuO_4$ and Pr_2CuO_4 is shown in Figs. 4 and 5, respectively. Pressure release revealed the same structural parameters as those upon increasing pressure (open symbols). This good agreement is an indication that the structural transitions are reversible. The V/V_0 data of the O-phase are also shown in these figures. The volume V of the unit-cell was divided by two to be comparable with the V/V_0 data of the tetragonal phases. The solid lines in these figures represent a fit of an equation of state (EOS) to the data. The Murnaghan EOS (25)

$$P(V) = \frac{B_0}{B_0'}\left\{\left(\frac{V_0}{V(P)}\right)^{B_0'} - 1\right\} \quad [1]$$

and the Birch EOS (26)

$$P(x) = \tfrac{3}{2} B_0\{x^{7/3} - x^{5/3}\}\{1 - \tfrac{3}{4}(4 - B_0')(x^{2/3} - 1)\} \quad [2]$$

with $x = V_0/V$ were used to check the consistency of the obtained fit parameters, the bulk modulus B_0 and its

TABLE 3
Tolerance Factor t, Unit-Cell Volume V_0 and V_T per Formula Unit at Ambient and the Transition Pressure P_T, c/a-Ratio at Ambient Pressure, as well as the Pressure Range where the T′- and T- (O- and T′-) Phase Coexist

Compound	t^a	V_0 (Å^3)	V_T (Å^3)	P_T (GPa)	c/a	T′-&T-phase	O-& T′-phase
La_2CuO_4	0.8684	95.15	92.67	3.4[b]	2.4491	—	—
$La_{1.4}Nd_{0.6}CuO_4$	0.8632	98.5	96.1	3.9	3.120(3)		
$La_{1.3}Nd_{0.7}CuO_4$	0.8623	98.2	95.2	5.6	3.116(3)		
$LaNdCuO_4$	0.8596	97.66	91.1	11.4	3.1109(2)	$11.4 < P < 15.0$ GPa	$2.3 < P < 10.6$ GPa
$La_{0.8}Nd_{1.2}CuO_4$	0.8579			7.0	3.103(4)		
$La_{0.5}Nd_{1.5}CuO_4$	0.8553			11.1	3.100(3)		
Nd_2CuO_4	0.8509	94.61	78.8	21.5	3.0866(9)	$21.5 < P < 29.5$ GPa	$10 < P < 18$ GPa
Pr_2CuO_4	0.8562	96.01	87.5	15.1	3.0900(2)	$P > 15.1$ GPa	$5.8 < P < 12.6$ GPa

Note. In addition to the measurements presented here other compounds of the solid-solution $La_{2-x}Nd_xCuO_4$ (12), of Nd_2CuO_4 (13), and La_2CuO_4 (23) are given. At low pressure and ambient temperature La_2CuO_4 attains the O-phase.

[a] Ionic radii for Cu^{2+} and O^{2-} in sixfold and Ln^{3+} in ninefold coordination (24).

[b] Transition pressure into the T-phase.

pressure dependence B'_0. The obtained volume compressibilities $\kappa_V = \partial V/(V_0 \partial P)$ are listed in Table 4 together with the a- and c-axis compressibilities κ_a and κ_c, defined in the same way. The values are the average of those obtained by Eq. [1] and [2].

The T′-structure is more compressible along the c-axis than along the a-axis, already visible in the insets of Figs. 4 and 5. This becomes more clear if the c/a-ratio is plotted versus pressure (Fig. 6). For comparison, the c/a-ratio of Nd_2CuO_4 (13) is included, too. Pressure reduces the

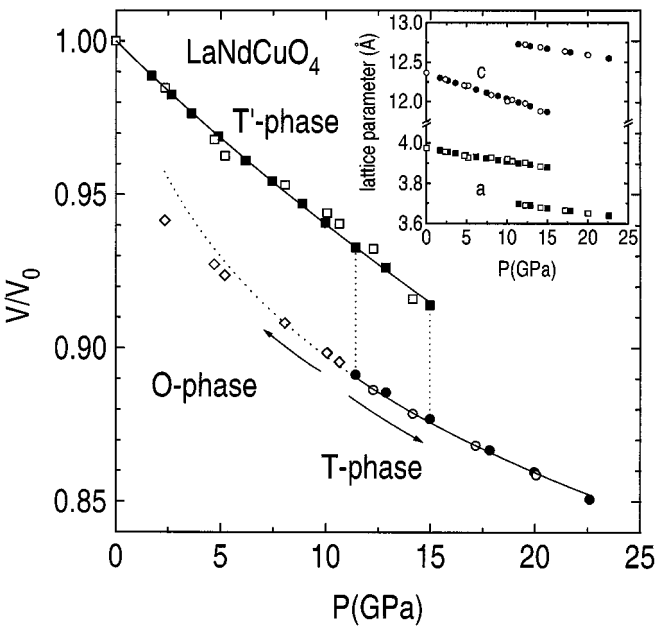

FIG. 4. Relative unit-cell volume V/V_0 of $LaNdCuO_4$ versus pressure. The solid lines represent a fit of an EOS to the data. The structural transformation into the high pressure T-phase starts at $P = 11.4$ GPa and is finished at $P = 15.0$ GPa. During pressure release (open symbols) the orthorhombic O-phase (open diamonds) occurs. The dotted line is the extension of the EOS of the T-phase. In the inset the pressure dependence of the a- and c-axis in the T′- and T-phase is shown for increasing (decreasing) pressure by solid (open) symbols.

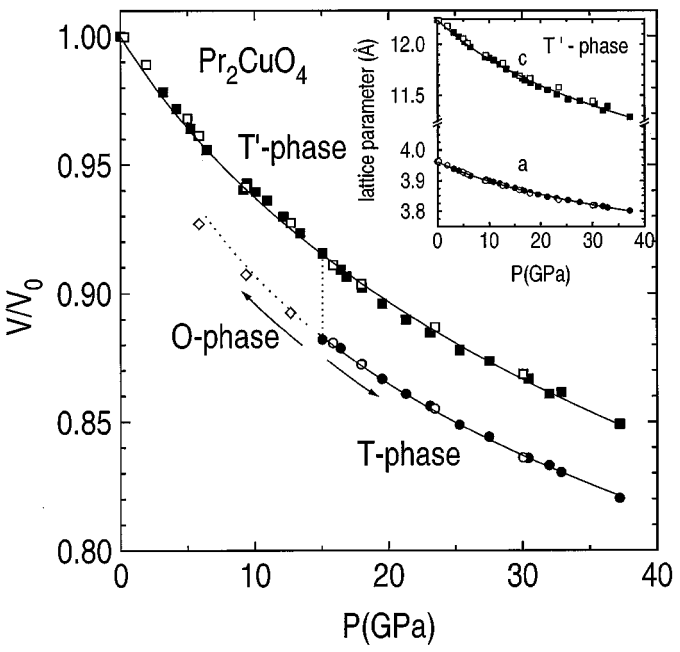

FIG. 5. Pressure dependence of the relative unit-cell volume V/V_0 of Pr_2CuO_4. The solid lines represent a fit of an EOS to the data. The structural transformation into the T-phase starts at $P_T = 15.1$ GPa. At the highest pressure still 50% of the T′-phase is present. During pressure release (open symbols) the orthorhombic O-phase (open diamonds) occurs. The dotted line is the extension of the EOS of the T-phase. In the inset the pressure dependence of the lattice parameters in the T′-phase is shown. Open symbols represent data obtained during pressure release.

TABLE 4
Compressibilities of the Lattice Parameters, Unit-Cell Volume, Some Interionic Distances, and the *c*/*a*-Ratio of Nd_2CuO_4, $LaNdCuO_4$, and Pr_2CuO_4 in the T′-Structure

	Nd_2CuO_4		$LaNdCuO_4$		Pr_2CuO_4		La_2CuO_4	
	exp. [13]	cal.	exp.	cal.	exp. [21]	cal.	exp. [6]	cal.
$\kappa_a = (10^{-3}\ \mathrm{GPa}^{-1})$	− 1.9(1)	− 1.9	− 1.9(2)	− 2.0	− 2.0(1)	− 2.0	− 2.2	− 2.5
$\kappa_b = (10^{-3}\ \mathrm{GPa}^{-1})$	− 1.9(1)	− 1.9	− 1.9(2)	− 2.0	− 2.0(1)	− 2.0	− 4.2	− 2.5
$\kappa_c = (10^{-3}\ \mathrm{GPa}^{-1})$	− 3.0(1)	− 3.8	− 3.0(1)	− 3.9	− 3.7(2)	− 3.8	− 1.8	− 2.5
$\kappa_V = (10^{-3}\ \mathrm{GPa}^{-1})$	− 6.9(1)	− 7.7	− 7.0(1)	− 7.9	− 7.9(5)	− 7.8	− 8.2	− 7.5
B_0 (GPa)	145(2)	131	143(1)	127	126(2)	129	122(2)	134
B'_0	4.1(4)	—	4.0(4)	—	5.0(6)	—	4	—
$\kappa_{Ln\text{–}O(2)}$ $(10^{-3}\ \mathrm{GPa}^{-1})$	− 1.8(2)	—	− 2.1(1)	—	− 2.7(2)	—		
$\kappa_{Ln\text{–}O(1)}$ $(10^{-3}\ \mathrm{GPa}^{-1})$	− 2.9(1)	—	− 3.2(1)	—	− 2.4(2)	—		
$\kappa_{Cu\text{–}O(2)}$ $(10^{-3}\ \mathrm{GPa}^{-1})$	− 2.8(1)	—	− 2.7(1)	—	− 3.2(3)	—		
$\kappa_{c/a}$ $(10^{-3}\ \mathrm{GPa}^{-1})$	− 1.0	—	− 1.0	—	− 1.4	—	+ 0.3	—

Note. Numbers in parentheses represent standard deviations of the last digit. According to a model described in the text the axis and volume compressibilities were calculated. In the last column data for La_2CuO_4 obtained by neutron measurements (6) ($P < 0.61$ GPa) are given.

c/*a*-ratio in all three compounds but the reduction is significantly larger (40%) in Pr_2CuO_4 (see Table 4). In the T-phase however, the *c*/*a*-ratio of all three compounds increases linearly with almost the same pressure coefficient. The *c*/*a*-values are of the same order as that of La_2CuO_4 (Table 4).

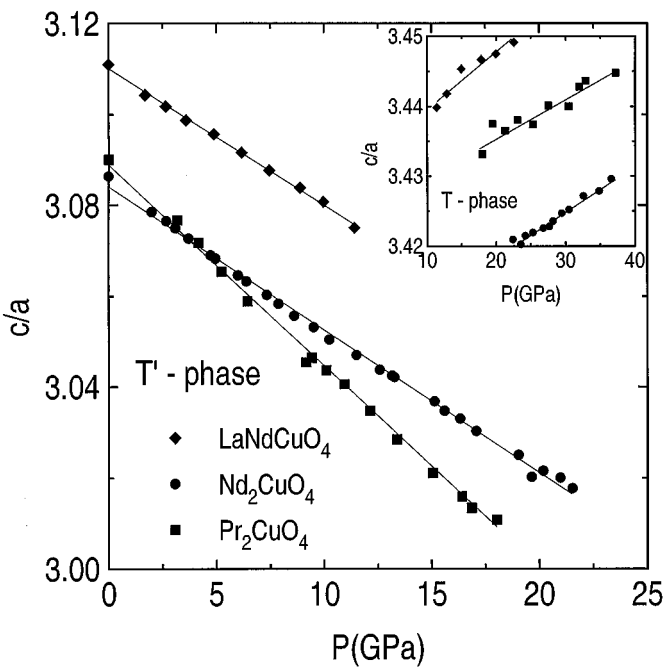

FIG. 6. The pressure dependence of the *c*/*a*-ratio of $LaNdCuO_4$, Nd_2CuO_4, and Pr_2CuO_4 in the T′-phase up to P_T. A stronger pressure dependence of *c*/*a* is seen for Pr_2CuO_4 in comparison to the other compounds. The inset shows the *c*/*a*-ratio for the T-phase, where all compounds show a similar increase in *c*/*a*.

This behavior is intuitively obvious as the crystal structure is regarded (Fig. 1). In the low-pressure phase the *Ln*–Cu distance along the *c*-axis is rather long and allows an easier compression along this direction than in the (*a*, *b*)-plane, due to the strong direct repulsion between the O(2) ions. The $[CuO_6]$ octahedra in the T-structure, however, are elongated along the *c*-axis to reduce the strain build up along the *a*-axis by the external pressure.

The only free parameter in the T′-structure is the fractional coordinate z_{Ln} of the lanthanide ion. It hardly changes in $LaNdCuO_4$ and Pr_2CuO_4 (Figs. 7a and 7b). In the high-pressure phase a slightly larger z_{Ln} value is found which also shows a negligible pressure dependence. In the T-phase the fractional coordinate $z_{O(2)}$ is an additional free parameter (Figs. 7c and 7d). In the case of Pr_2CuO_4 an increase of $z_{O(2)}$ is observed. A similar increase of $z_{O(2)}$ was observed in the two phase domain of Nd_2CuO_4 (13). The coexistence of the T′- and T-phase in $LaNdCuO_4$ is limited to a small pressure range ($11.4 \leq P \leq 15.0$ GPa). From the three patterns recorded in this domain no clear picture of the pressure dependence of $z_{O(2)}$ can be drawn. It seems likely that $z_{O(2)}$ changes with pressure similarly to how it does in the other two compounds.

Upon decreasing pressure the intermediate orthorhombic structure was attained in all three compounds as pressure became lower than P_T. The initial T′-structure was eventually obtained at pressures below 10, 5.8, and 2.3 GPa for Nd_2CuO_4, Pr_2CuO_4, and $LaNdCuO_4$, respectively. In the case of $LaNdCuO_4$ the O-phase occurred in a rather large pressure interval ($2.3 < P < 10.6$ GPa). Therefore, detailed structural information of this phase could be obtained. During pressure release the orthorhombic distortion, defined as the difference between the *c*- and *a*-axis normalized

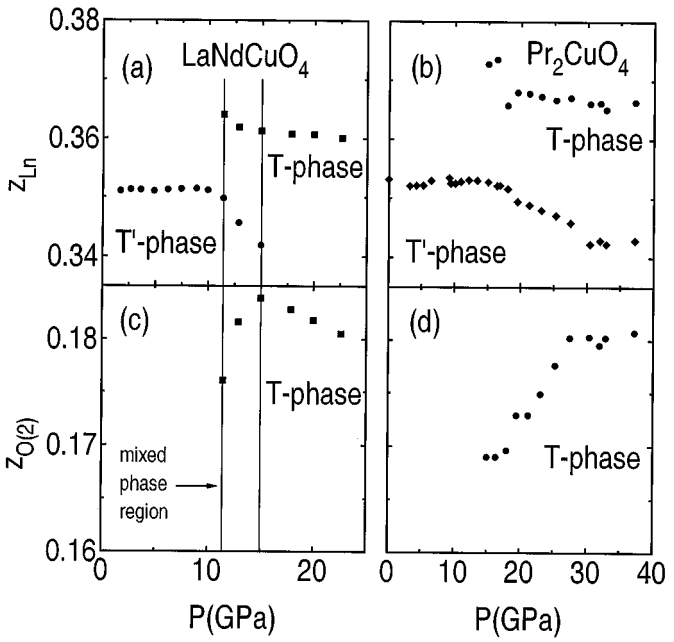

FIG. 7. Fractional coordinates z_{Ln} and $z_{O(2)}$ of the lanthanide and O(2)-ions in the T′-, and T-structure as function of pressure for $LaNdCuO_4$ (left panel) and Pr_2CuO_4 (right panel). In $LaNdCuO_4$ a two phase region (T′- and T-phase) is found between 11.4 GPa and 15.0 GPa. For Pr_2CuO_4 the high pressure T-phase becomes detectable above 15.1 GPa but the T′-phase fraction dominates.

in respect to the a-axis, increases gradually in all the systems (see Fig. 8). Simultaneously, the basal plane of the octahedron is rotated around the [100] direction. The rotation angle decreases continuously (7° at 8.5 GPa to 3° at 2.5 GPa). Furthermore, the $[CuO_6]$ octahedra are distorted in the sense that the apical oxygen is shifted away from the fourfold rotation axis of the parent T-phase structure. All Ln–O distances increase as pressure is lowered which reflects in a certain way the decrease in the octahedral tilt and distortion. Regarding the resemblance of the sequence of the structural transformations, it is likely that such structural changes also might occur in the other members of the $La_{2-x}Nd_xCuO_4$ solid solution.

4. DISCUSSION

4.1. Compressibility of the Structure

The anisotropic compressibilities of the lattice parameters and the volume can be calculated following a simple model introduced by Cornelius and co-workers (27). In the T′-structure the cations M = Cu and Ln (Ln = La, Nd, or Pr) have an eightfold oxygen coordination. Thus, the unit-cell can be built up with $[MO_8]$ polyhedra. For each polyhedron the mean M–O distance defines an average bond length $d_{M\text{-O}}$. Hazen and Finger (28) reviewed many oxides, in particular those with the cubic rocksalt structure, and found the empirical expression $\kappa_V^{poly} = 3\kappa_{M\text{-O}}^{poly}$ for the volume compressibility κ_V^{poly} of the polyhedron and the linear compressibility $\kappa_{M\text{-O}}^{poly}$ of the distance $d_{M\text{-O}}$. The latter is given by

$$\kappa_{M\text{-O}}^{poly} = 0.44\frac{d_{M\text{-O}}^3}{Z_M} \times 10^{-3}, \qquad [3]$$

where Z_M is the valence of the cation M. In this relation $\kappa_{M\text{-O}}^{poly}$ is in GPa^{-1} and d in Å. Following the description of Ref. (27) the unit cell of the T′-structure contains $[LnO_8]$ polyhedra and $[CuO_8]$ boxes. The latter are formed by the Cu–O(1) plane and the plane of the four O(2) ions. The polyhedra contain four Ln–O(1) and Ln–O(2) distances ($\approx$2.68 Å and $\approx$2.32 Å, respectively). In the boxes four Cu–O(1) bonds and four Cu–O(2) distances ($\approx$1.97 Å and $\approx$3.62 Å, respectively) are present. The $[CuO_8]$ boxes are more rigid in the basal plane (Cu–O(1) bond) than perpendicular to it (large Cu–O(2) distance). With the assumption that the $[MO_8]$ polyhedra are compressed isotropically the compressibilities of the crystal can be calculated. Since the two polyhedra each fill half the volume, the compressibilities κ_a and κ_c along the a- and c-axis as well as the volume compressibility κ_V are given by

$$\kappa_a^{-1} = \tfrac{1}{2}(\kappa_{Ln\text{-O}}^{-1} + \kappa_{Cu\text{-O}(1)}^{-1}), \qquad [4]$$

$$\kappa_c^{-1} = \tfrac{1}{2}(\kappa_{Ln\text{-O}}^{-1} + \kappa_{Cu\text{-O}(2)}^{-1}), \qquad [5]$$

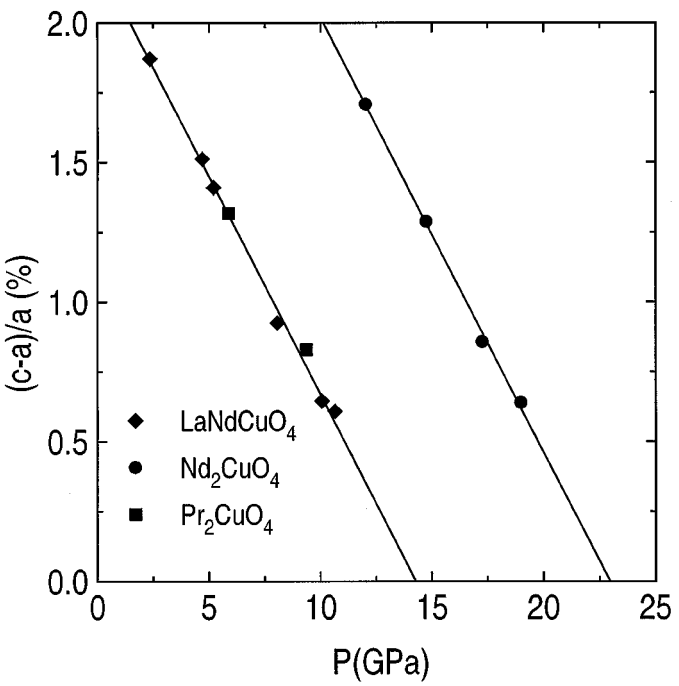

FIG. 8. Pressure dependence of $(c-a)/a$ in the O-phase which is a measure of the deviation from the tetragonal symmetry. In all three compounds this value increases similarly.

and

$$\kappa_V = 2\kappa_a + \kappa_c. \quad [6]$$

Substituting the distances, which can be deduced from Tables 1 and 2 and the table of Ref. (13), into Eqs. [3]–[6] the compressibilities and the bulk moduli of $LaNdCuO_4$, Pr_2CuO_4, and Nd_2CuO_4 can be calculated (Table 4). The agreement to the measured values of κ_a and κ_V is in all cases better than 4% and 12%, respectively. The large uncertainty in the latter is due to κ_c, which is about 20% higher than the measured values for the $La_{2-x}Nd_xCuO_4$ compounds with $x = 1$ and 2. A good agreement (better than 3%) is obtained for Pr_2CuO_4. A similar approach can be made to calculate the compressibilities for the O-phase of La_2CuO_4. Following the same procedure as just described, the values for La_2CuO_4, given in Table 4, were found. Also in this case the experimental values (apart from κ_b) are reasonably well reproduced. However, the calculated values reveal an isotropic compression whereas the experimental data show a highly anisotropic behavior along the *a*- and *b*-axis.

From a crystal-chemistry point of view the model used here is only a crude approximation despite its good agreement with the measured values. The Cu–*Ln* distance ($d < 2.79$ Å) is much shorter than the Cu–O(2) distance ($d = 3.62$ Å) and this is not accounted for in Eq. [3]. Therefore, it is expected that this makes the structure more rigid along the *c*-axis than it is calculated. Furthermore, the compressibility κ_V is a combination of polyhedral compression and bond bending (28) especially in the orthorhombic structure of La_2CuO_4.

The compression of several *M*–O distances is also reported in Table 4. In the $La_{2-x}Nd_xCuO_4$ solid solution the *Ln*–O(2) and *Ln*–O(1) distances vary like the *a*- and *c*-axis compressibilities, respectively. This is not surprising because the only way to diminish the internal stress is to decrease the largest *Ln*–O distance (i.e., *Ln*–O(1)). The compressibility of the remaining two Cu–O distances is the same as κ_a (for Cu–O(1)) and κ_c (for Cu–O(2)). These observations show that κ_a and κ_c are determined by the pressure dependence of the *Ln*–O(2) and Cu–O(1) and the *Ln*–O(1) and Cu–O(2) distances, respectively. The values given in Table 4 for Nd_2CuO_4 are in good agreement to data obtained by neutron measurements (29).

In Pr_2CuO_4 κ_a is the same as for the other two compounds but κ_c is significantly higher. This is nicely reproduced in the model calculations and agrees qualitatively with the data of Ref. (30) if they are shifted by 25%. However, it seems that the correlation between axis compressibility and the pressure dependence of *Ln*–O distances found for the other two compounds is not valid in Pr_2CuO_4: The Pr–O(2) distance is more compressible than the *a*-axis and the Pr–O(1) distance is significantly stiffer than the *c*-axis. The origin of this difference might be related to the Pr ion, since the rare earth ion is the only difference to the $LaNdCuO_4$ compound, where the interionic distances are comparable.

4.2 Structural Evolution with Pressure

The crystal structure of these materials has several important crystal-chemical features in common. The CuO_2 planes, where the superconductivity is believed to occur in the doped compounds, alternate with other layers. In this intergrowth structure a single CuO_2 plane alternates for example with a $(LaO)_2$ rocksalt layer in the O-structure of La_2CuO_4. However, above 530 K (31) the $[CuO_6]$ octahedra are no longer tilted about the [110] direction and the T-structure is found.

The influence of high pressure on the T′-structure can be understood qualitatively in considering the coordination number of the rare earth ions and the density of the structure. As pressure is applied the density increases and a higher coordination number is favored according to the pressure-coordination rule (32). Hence, the $T' \rightarrow O$ transition is likely to occur. In the O- and T-structure the Ln^{3+} and Cu^{2+} ions have a ninefold (mono-caped quadratic antiprism) and sixfold (elongated octahedron) coordination, respectively (Figs. 1b and 1c). In the T′-structure however, the Ln^{3+} and Cu^{2+} ions occupy an eightfold (pseudo-cubic) and fourfold (square-planar) coordinated site, respectively, where only the O(2) ions have changed position (Fig. 1a). The structure is built up from an arrangement of fluorite-like *Ln*O layers and CuO_2 planes. But to understand the observed increase in P_T as *t* decreases we have to look at the $La_{2-x}Nd_xCuO_4$ phase diagram and especially at the *Ln*–O(2) and O(2)–O(2) interactions.

The stability of the different structures requires a bond-length matching between adjacent layers and is evaluated in terms of the Goldschmidt tolerance factor

$$t = (r_{Ln^{3+}} + r_{O^{2-}})/\sqrt{2}(r_{Cu^{2+}} + r_{O^{2-}}), \quad [7]$$

where $r_{Ln^{3+}}$, $r_{Cu^{2+}}$, and $r_{O^{2-}}$ are the ionic radii of the lanthanide, the copper, and the oxygen ions, respectively (33, 34). For the sake of consistency, the *t* values of the T′- and O-structure are calculated using rare earth ions in a ninefold and copper and oxygen ions in a sixfold coordination (see Table 3). For the $La_{2-x}Nd_xCuO_4$ solid-solution the following phase diagram under normal conditions has been obtained (35, 36) : (i) the T-structure exists for $0.99 \geq t \geq 0.88$, (ii) the O-structure is present for $0.88 > t \geq 0.865$, (iii) the T′-structure is stable for $0.865 > t \geq 0.83$, and (iv) for $0.83 > t$ a mixture of Ln_2O_3 and a new compound with the formula $Ln_2Cu_2O_5$ was found (36, 37). A treatment of this mixture at high pressure and high temperature, however, has allowed the stabilization the T′-structure down to $t = 0.814$ (for *Ln* = Tb, Dy, Ho, Er, Tm) (38).

In the O-structure compressive and tensile forces are present in the basal CuO_2 plane and the $(LnO)_2$ rocksalt-like layer, respectively. For La_2CuO_4 the interionic Cu–O(1) distances ($a/2 \approx 1.91$ Å) are shorter than the sum of the ionic radii (2.13 Å, with $r_{Cu^{2+}} = 0.73$ Å and $r_{O^{2-}} = 1.40$ Å; in this work Shannon's ionic radii (24) are used) which leads to a compression. However, the two Cu–O(2) distances are significantly longer (2.46 Å, using $c = 13.15$ Å (36, 39)). The tension is due to the fact that eight out of nine *Ln*–O interionic distances are longer (≈ 2.64 Å for *Ln*–O(1) and ≈ 2.77 Å for *Ln*–O(2)) and only the distance between the lanthanide and the apical oxygen (≈ 2.30 Å) is shorter than the sum of the ionic radii (2.62 Å, using $r_{La^{3+}} = 1.216$ Å). Both kinds of stresses are partially relieved by a cooperative tilting of the octahedra, resulting in the orthorhombic distortion (i.e., the T → O transition).

The average lanthanide ionic radius

$$r_{Ln^{3+}} = 0.5[(2 - x)r_{La^{3+}} + xr_{Nd^{3+}}] \qquad [8]$$

decreases by Nd substitution ($r_{Nd^{3+}} = 1.163$ Å). Hence, by definition the tolerance factor t decreases, too. When the critical value $t = 0.865$ is reached, the O(2) ions move from the 4*e* site of the O-structure (0,0,*z*; 0,0, $-z$) to the 4*d* site ($0,\frac{1}{2},\frac{1}{4}$; $\frac{1}{2},0,\frac{1}{4}$) of the T′-structure (see Fig. 1). The O → T′ transition as a function of the average lanthanide ion size has been interpreted as optimization of the *Ln*–O distances (34, 35, 36). The average *Ln*–O distance in the T′-structure is significantly shorter (2.51 Å instead of 2.64 Å) in the resulting fluorite-like arrangement compared to the rock salt-like layer in the O-structure. Among the eight *Ln*–O distances in the T′-structure four are significantly shorter (2.32 Å, for *Ln*–O(2)) and four are longer (2.68 Å, for *Ln*–O(2)) than the sum of the ionic radii. Therefore, a compression in the *Ln*–O(2) linkages is present. Furthermore, the oxygen ions at the 4*d* site are separated only by $a/\sqrt{2}$ (≤ 2.81 Å), which is close to the sum of the ionic radii (2.80 Å). The structure has to expand in the basal plane of the tetragonal structure to diminish the O(2)–O(2) repulsion. As a consequence the CuO_2 layers in the T′-structure are under tension. The expansion in the basal plane is not compensated by a sufficient decrease in the *c*-parameter which hence results in a considerably larger unit-cell volume as compared to the O-structure. Considering the smaller average rare earth size this is not expected.

In Fig. 9 the transition pressure P_T is plotted versus the tolerance factor t. We have chosen t as variable because it takes the *Ln*–O and Cu–O ionic bonding into account and gives an estimate of the structural stability. Nevertheless, the Nd content x can also be used. According to the definitions of t and the average radius $r_{Ln^{3+}}$, a linear relation between t and x exists. Fitting the data to a linear $P_T(t)$-dependence (solid line in Fig. 9) and extrapolating it to zero pressure

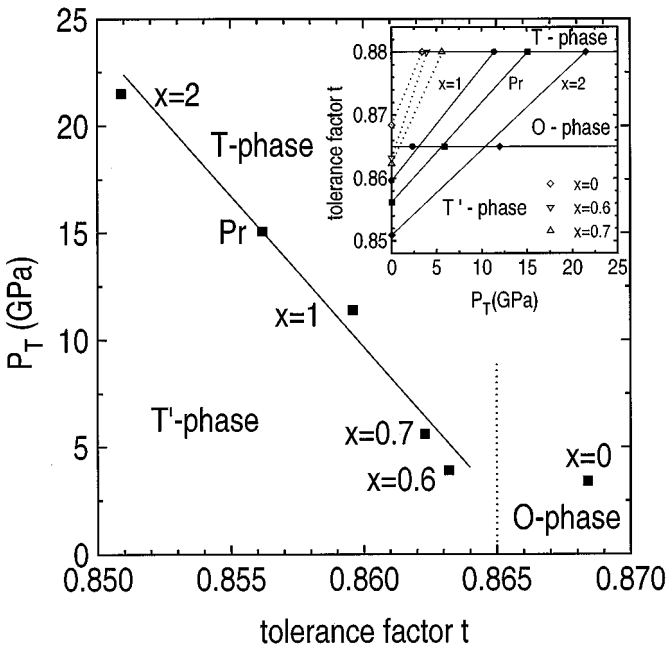

FIG. 9. Transition pressure P_T versus the tolerance factor t for $La_{2-x}Nd_xCuO_4$ compounds and Pr_2CuO_4. The straight line separates the T′- and T-phase. Above $t = 0.865$ the orthorhombic O-phase is the stable low pressure phase. The point shown in this region represents La_2CuO_4 which transforms into the T-phase at 3.4 GPa. The tolerance factor t versus the transition pressure P_T is plotted in the inset. Points at the $t = 0.865$ (0.88) line represent the lowest pressures where the T-(O-)phase was observed.

yields $t = 0.8662$. This value is only slightly higher than $t = 0.865$ which represents the border of stability of the T′ structure, indicated by the vertical dotted line in Fig. 9.

An interesting insight in the phase sequence can be obtained if the tolerance factor is plotted versus the transition pressure P_T (inset Fig. 9). The symbols at ambient pressure are the starting tolerance factor of the various compounds. The corresponding points at the $t = 0.88$ line represent the transition pressure P_T found in the $La_{2-x}Nd_xCuO_4$ compounds (12, 13) and Pr_2CuO_4 (21). Assuming a linear $t(P)$ relation, the line between the $t(P = 0)$ and $t(P_T)$ points gives for each compound an intersection with the $t = 0.865$ line. This line represents the lower limit of the O-phase. The points plotted at this line represent the lowest pressure values where the O-phase was still observed in the diffraction patterns during pressure release. A good agreement is found between these experimental transition pressures and the intersection of the linear $t(P)$ dependence and the $t = 0.88$ line. That the intermediate O-phase is not observed during increasing pressure and there exists a large T′- and T-phase domain (more than 25 GPa in the case of Pr_2CuO_4) are likely due to some hysteresis in the phase transitions, since the experiments were carried out at ambient temperature. This phenomenon is less pronounced during decreasing pressure, and the observed phase sequence

$T \rightarrow O \rightarrow T'$ shows clearly how pressure is able to tune the value of the tolerance factor t.

The reversibility of the transition proves that the T-structure is not induced by a change in composition, but results only from the pressure effect. This is also confirmed by the crystal structure refinement of the synchrotron X-ray data.

5. CONCLUSION

The pressure-induced structural changes in $LaNdCuO_4$ and Pr_2CuO_4 up to 37 GPa have been investigated by synchrotron radiation at ambient temperature. The low-pressure T′-structure ($I4/mmm$, Nd_2CuO_4-type) transforms into the T-structure ($I4/mmm$, K_2NiF_4-type) at $P_T = 11.4$ and 15.1 GPa, respectively. During pressure release both compounds attain in a certain pressure range the orthorhombic O-phase (*Cmca*, distorted K_2NiF_4-type) and the structure transforms eventually into the initial T′-structure at low pressures. In combination with previous results obtained on other members of the solid solution $La_{2-x}Nd_xCuO_4$ P_T decreases linearly with the tolerance factor t and increases linearly with x. This behavior is related to compressive stress in the Ln–O(2) linkages in the fluorite-like LnO_2 layers. The compressive stress decreases when the average lanthanide ion size is reduced, i.e., $x \rightarrow 2$. As a consequence, higher pressure is necessary to induce the structural transition. The axis and volume compressibilities can be well described by a simple model in which different polyhedra and their linear compressibilities are considered. The Cu–O(1) bond and the Cu–O(2) distance (T′-phase) show the same compressibility as the a- and c-axis, respectively. These experiments show that a pressure-induced $T' \rightarrow T$ transition upon pressure increase and a $T \rightarrow O \rightarrow T'$ phase sequence during pressure release is likely to occur in the $La_{2-x}Nd_xCuO_4$ solid solution for all x in the range $0.6 \leq x \leq 2$.

ACKNOWLEDGMENTS

We acknowledge many fruitful discussions with Dr. H. Kohlmann.

REFERENCES

1. B. Dabrowski, Z. Wang, K. Rogacki, J. D. Jorgensen, R. L. Hitterman, J. L. Wagner, B. A. Hunter, P. G. Radaelli, and D. G. Hinks, *Phys. Rev. Lett*. **76,** 1348 (1996).
2. H. Casalta, P. Bourges, M. d'Astuto, D. Petitgrand, and A. Ivanov, *Phys. Rev. B* **57,** 471 (1998).
3. J.-S. Zhou, J. B. Goodenough, H. Sato, and M. Naito, *Phys. Rev. B* **59,** 3827 (1999).
4. N. Yamada and M. Ido, *Physica C* **203,** 240 (1992).
5. J.-S. Zhou, H. Chen, and J. B. Goodenough, *Phys. Rev. B* **49,** 9084 (1994).
6. H. Takahashi, H. Shaked, B. A. Hunter, P. G. Radaelli, R. L. Hitterman, D. G. Hinks, and J. D. Jorgensen, *Phys. Rev. B* **50,** 3221 (1994).
7. Y. Tokura, H. Takagi, and S. Uchida, *Nature* **337,** 345 (1989).
8. N. M. Pyka, A. Metz, M. Loewenhaupt, and R. van de Kamp, *Physica B* **241–243,** 865 (1998).
9. J. W. Lynn, I. W. Sumarlin, S. Skanthakumar, W.-H. Li, R. N. Shelton, J. L. Peng, Z. Fisk, and S.-W. Cheong, *Phys. Rev. B* **41,** 2569 (1990).
10. T. Brugger, T. Schreiner, G. Roth, P. Adelmann, and G. Czjek, *Phys. Rev. Lett*. **71,** 2481 (1993).
11. P. Fulde, V. Zevin, and G. Zwicknagl, *Z. Phys. B* **92,** 133 (1993).
12. H. Wilhelm, C. Cros, F. Arrouy, and G. Demazeau, *J. Solid State Chem.* **126,** 88 (1996).
13. H. Wilhelm, C. Cros, E. Reny, G. Demazeau, and M. Hanfland, *J. Mater. Chem.* **8,** 2729 (1998).
14. J. Piermarini, S. Block, J. D. Barnett, and R. A. Forman, *J. Appl. Phys.* **46,** 2774 (1975).
15. H. K. Mao, P. M. Bell, J. W. Shanner, and D. J. Steinberg, *Appl. Phys.* **49,** 3276 (1978).
16. H. K. Mao, J. Xu, and P. M. Bell, *J. Geophys. Res.* **91,** 4673 (1986).
17. A. P. Hammersly, ESRF Internal Report EXP/AH/95-01 (1995).
18. A. C. Larson, GSAS manual, LAUR 86-748 (1986).
19. M. Hanfland, M. Lorenzen, C. Wassilew-Reul, and F. Zontone, *Rev. High Pressure Sci. Technol.* **7,** 787 (1998).
20. We use the standard *Cmca* setting for the O-phase rather than the *Bmab* setting. In this case the long lattice translation is along the *b*-axis. The *a*- and *c*-directions are each $\sqrt{2}$ times the *a*-axis of the tetragonal $I4/mmm$ setting (T′- or T-structure). Hence, the unit-cell volume is twice as large as the *I*-centered unit-cell volume. The $O \rightarrow T$ transition can be expressed in terms of crystallographic group-subgroup relationships. From the $I4/mmm$ structure a *translationengleiche* transition of index 2 leads to *Fmmm* and then a *klassengleiche* transition of index 2 leads to *Cmca*.
21. H. Wilhelm, C. Cros, E. Reny, G. Demazeau, and M. Hanfland, *Rev. High Pressure Sci. Technol.*, in press.
22. A similar table was presented for Nd_2CuO_4 in Ref. (13). In this table two typing errors occured. First, the temperature factor U of the O(2)-ion in the T-phase at 21.5 GPa has to be $2.6(1) \times 10^{-2}$ Å^2. Second, the fractional coordinate y/b of the O(1)-ion in the O-phase at 17.3 GPa has to be 0.34(1).
23. J. Shu, J. Akella, J. Z. Liu, H. K. Mao, and L. Finger, *Physica C* **176,** 503 (1991).
24. D. Shannon, *Acta Crystallogr. Sect. A* **32,** 751 (1976).
25. F.D. Murnaghan, *Proc. Natl. Acad. Sci.* **30,** 244 (1944).
26. F. Birch, *Phys. Rev.* **47,** 809 (1947).
27. A. L. Cornelius, S. Klotz, and J. S. Schilling, *Physica C* **197,** 209 (1992).
28. R. M. Hazen and L. W. Finger, "Comparative Crystal Chemistry." Wiley, Chichester, 1982.
29. T. Kamiyama, F. Izumi, H. Takahashi, J. D. Jorgensen, D. Dabrowski, R. L. Hitterman, D. G. Hinks, H. Shaked, T. O. Mason, and M. Seabaugh, *Physica C* **229,** 377 (1994).
30. W. H. Fietz, C. A. Wassilew, D. Ewert, M. R. Dietrich, H. Wühl, and D. Hochheimer, *Phys. Lett. A* **142,** 300 (1989).
31. R. J. Birgenau, C. Y. Chen, D. R. Gabbe, H. P. Jenssen, M. A. Kastner, C. J. Peters, P. J. Picone, T. Thio, T. R. Thurton, and H. L. Muller, *Phys. Rev. Lett*. **59,** 1329 (1987).
32. A. Neuhaus, *Chimia* **18,** 93 (1964).
33. V. M. Goldschmidt, *Akad. Oslo I. Mater. Natur.* **2,** 7 (1926).
34. P. Ganguly and C. N. Rao, *J. Solid State Chem.* **53,** 193 (1984).
35. A. Manthiram and J. B. Goodenough, *J. Solid State Chem.* **87,** 402 (1990).
36. J. F. Bringley, S. S. Trail, and B. A. Scott, *J. Solid State Chem.* **86,** 310 (1990).
37. N. Kimizuka, E. Takayama, and S. Horiuchi, *J. Solid State Chem.* **42,** 322 (1962).
38. H. Okada, M. Takano, and Y. Takeda, *Physica C* **166,** 111 (1991).
39. B. Grande, H. Müller-Buschbaum, and M. Schweitzer, *Z. Anorg. Allg. Chem.* **428,** 120 (1977).